JOURNAL OF GEOPHYSICAL RESEARCH, VOL. 104, NO. B1, PAGES 725–736, JANUARY 10, 1999

Collection and three-dimensional modeling of GPS and tilt data at Merapi volcano, Java

François Beauducel and François H. Cornet

Laboratoire de Mécanique des Roches, Département de Sismologie, Unités Mixtes de Recherche CNRS, Institut de Physique du Globe de Paris, Paris, France

Abstract. We study here the deformations associated with the November 1996 to March 1997 eruption period at Mount Merapi (Central Java), one of the most active volcanoes in Indonesia. This activity period includes a vertical explosion on January 17 and an increase of the lava dome volume by about 3×10^6 m^3. Two Global Positioning System (GPS) campaigns have been carried out on a six-benchmark network at the beginning and at the end of the period. Relative displacements with respect to the reference point show an average subsidence of 6.5 cm. A multicomponent tilt station installed on the southeast flank, 3 km from the summit, recorded a tilt of 11.1 ± 0.7 μrad in the tangential direction and 0.9 ± 0.4 μrad in the radial direction. These data are interpreted using a three-dimensional (3-D) elastic model based on the mixed boundary element method and a near-neighbor Monte Carlo inversion. Interpretation of tilt data requires an accurate mesh for discretizing the 3-D topography. The final result supports a horizontal elliptic magma source located 8.5 ± 0.4 km below the summit and 2 ± 0.4 km to the east of it. In particular, the data cannot be consistent with the location of a magma chamber determined from seismic activity analysis (i.e., 2 km below the summit). The computed depth depends strongly on the source shape and cannot be constrained properly because of the small amount of data. The computed deflation of $11 \pm 2\times10^6$ m^3 is about 3 times larger than the observed increase in the lava dome volume. This difference is attributed to rock avalanches and pyroclastic flows on the flanks of the volcano.

1. Introduction

Some understanding of magma conduits in volcanoes can be achieved from seismic tomography, gravity, or magnetic fields analysis. The study of ground deformations (displacements, tilt, and strain) also contributes to this understanding, but it requires observations before and after eruption periods of interest. Recent synthesis of volcano geodesy has been conducted by *Dvorak and Dzurisin* [1997]. One of their main conclusions is that geodesy yields estimates of magma supply rates, the location of sources, and, in some cases, the size and shape of complex magma reservoirs. This has been done only at a few dozen of the world's 600 active volcanoes.

In this paper, we address Mount Merapi, an andesitic stratovolcano located on Central Java, Indonesia (see Figure 1). Since 1992, Merapi experienced quasi-continuous extrusion of lava at its summit, which forms a dome in a horseshoe-shaped crater. The dome is continuously and partially destroyed by avalanches and pyroclastic flows [*Tjetjep and Wittiri*, 1996]. During the period November 1996 to March 1997 (about 150 days), the lava dome grew by about 3.2×10^6 m^3, while 126 pyroclastic flows and 16,200 rock avalanches have been recorded (see Figure 4b). On January 17, 1997, at 1034 LT (UT+7), a vertical explosion occurred, forming an eruption column more than 4 km high. The explosion destroyed at least 1.3×10^6 m^3 of the existing dome (A. Ratdomopurbo, personnal communication, 1997). The growth rate of the dome corresponds exactly to the long-term average of lava production at Merapi which is equal to 20,000 m^3 d^{-1} [*Allard et al.*, 1995].

We present here an analysis of this 5-month eruption period, based on two types of observations: (1) Global Positioning System (GPS) data measured at the beginning and at the end of the period, and (2) continuous tilt variation signals recorded during the period. Looking for large-scale effects, we do not consider summit deformation data but concentrate on observations from the lower flanks of the edifice. In this domain, elasticity applies and a three-dimensional (3-D) model which takes into account both the real topography and the shape of the magma chamber is proposed. The best solution is sought for with a near-neighbor Monte Carlo inversion method.

2. GPS Measurements

The GPS network is based on existing benchmarks installed by the Volcanological Survey of Indonesia and U.S. Geological Survey for Electronic Distance Measurement (EDM) monitoring [*Subandriyo et al.*, 1995]. Figure 1 shows the positions of the six chosen points: reference point JRA0 (observation post Jrakah) located on the older Merbabu volcano, BAB0 (observation post Babadan), DEL1 (close to the tilt station Deles), SEL0 (Selokopo Atas), PUS0 (Pusunglondon) and LUL0 (Luluk) at the summit. These benchmarks are actually used as a first-order network for a 10-point GPS and microgravity summit network measured every year since 1993 [*Jousset et al.*, 1998; *Beauducel*, 1998].

The relatively short dimension of the network (8 km for the longest baseline) allows for the use of single-frequency receivers [*Botton et al.*, 1997]. Each campaign included 14 measurement sessions between every two benchmarks, with only two receivers

Paper number JGRB-1998900031.
0148-0227/99/JGRB-1998900031$09.00

(Sercel NR101). These sessions consisted of 2 to 6 hours of simultaneous recording, depending on the baseline length. Because of the number of receivers, the campaign spent about 3 weeks on the field, and sessions were carried out at different days and times that imply decorrelated ionospheric and tropospheric effects (no systematic error). The redundancy factor *f'*, as defined by *Botton et al.* [1997], is

$$f' = 0.9\frac{(r-1)s}{n-1}, \qquad (1)$$

where $r = 2$ is the number of receivers, $s = 14$ is the total number of sessions (baselines), and $n = 6$ is the number of benchmarks. This factor stands for a degree of confidence associated with point position determination. Our value $f' = 2.5$ is sufficient for a standard small network.

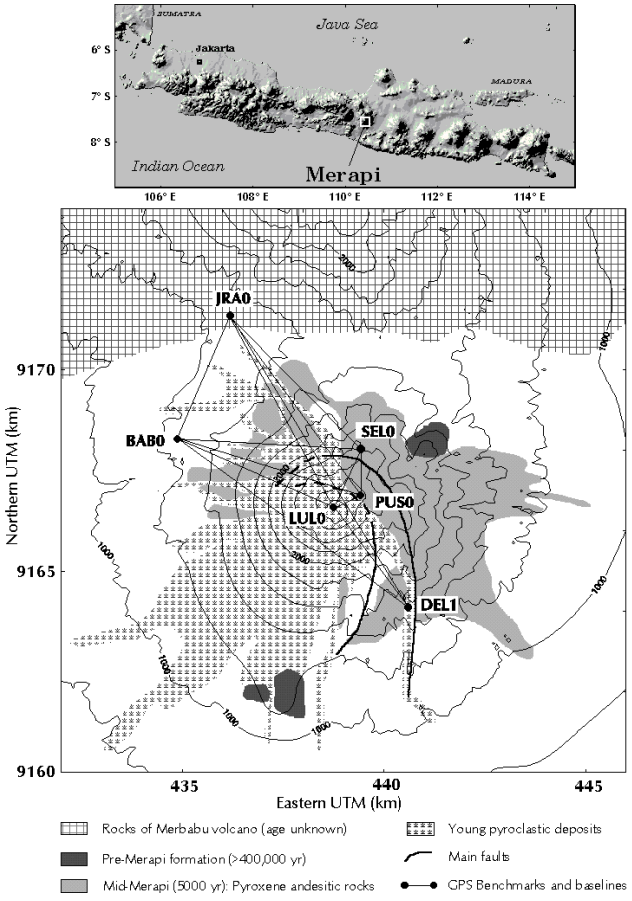

Figure 1. Location of Mount Merapi on Java Island, Indonesia, and schematic geologic map. Positions of Global Positioning System (GPS) benchmarks and baselines measured during each campaign are also indicated. Universal Transverse Mercator (UTM-49); JRA0 Jrakah; BAB0 Babadan; DEL1 Deles; SEL0 Selokopo Atas; PUS0 Pusunglondon; LUL0 Luluk. Tilt station Deles is installed at DEL1, on large pyroxene andesitic lava flows, capped by young pyroclastic deposits.

Because altitude differences between points are relatively large (up to 1600 m), a local meteorological model based on field measurements was used for baseline processing, in order to reduce tropospheric refraction effects [*Klein and Boedecker*, 1989; *Gurtner et al.*, 1989]. During each session, atmospheric pressure, dry temperature, and relative humidity were taken at each point every 15 or 30 min. Parameters were reduced to a single elevation according to the tropospheric vertical gradients for pressure (equation (2a)) [*Triplet and Roche*, 1983] and temperature at tropical areas (equation (2b)) [*Saastamoinen*, 1972]. We chose to use a constant value for relative humidity (equation (2c)), equal to the ground value, as suggested by *Baby et al.* [1988]:

$$P = P_0\,(1 - 0.0000226h)^{5.225} \qquad (2a)$$

$$T = T_0 - 0.00606h \qquad (2b)$$

$$H = H_0\,. \qquad (2c)$$

Wet temperature is then computed for all measurements through thermodynamic equations. Its daily variations show a small standard deviation of 2.6° (Figure 2). Therefore, we compute an average value for these three parameters (pressure, dry temperature, and relative humidity) for each time session. The software (Sercel GPSWin) determines the baselines by the double-difference method [*Dixon*, 1991], including meteorological data for tropospheric delay estimations [*Hopfield*, 1971]. Note that all integer ambiguities were fixed, which is not the case if we use a standard tropospheric model. For long baselines, only 2 or 3 hours of measurement have been selected and kept for the processing, by excluding periods that show large residues in double difference (probably owing to ionospheric effect). Baseline average errors stand for 1 to 2 cm in horizontal and 2 to 5 cm in vertical, which is commonly observed with single-frequency receivers (P. Segall, personnal communication, 1998).

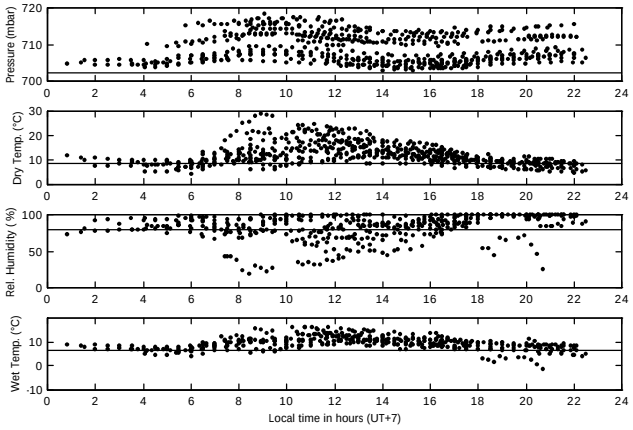

Figure 2. Meteorological data during both 1996 and 1997 GPS campaigns at Merapi. They have been reduced with respect to the 3000-m elevation (see text), and they are presented on a single-day scale in local time. Pressure, dry temperature, and relative humidity are field measurements at GPS points. Wet temperature is computed from thermodynamic equations. It shows a relative stability in time (standard deviation of 2.6 °C). Horizontal lines represent theoretical values for tropical area.

Table 1. September 1996 Coordinates and a Posteriori Errors for GPS Network Points

Point		Local coordinates UTM -49 WGS84, m			Errors a posteriori σ, m		
Number	Name	East	North	Up	*dE*	*dN*	*dU*
085	DEL1	440692.1316	9163972.9254	1511.4785	0.0241	0.0264	0.0456
090	BAB0	434975.8720	9168041.1995	1321.0498	0.0096	0.0079	0.0135
100	JRA0	436180.2839	9171235.4989	1335.4256	—	—	—
105	SEL0	439543.9619	9167528.3108	2570.4405	0.0068	0.0045	0.0088
107	PUS0	439552.3005	9166838.7134	2734.0199	0.0085	0.0062	0.0114
120	LUL0	438978.0716	9166537.5339	2976.7933	0.0074	0.0053	0.0105

Coordinates and a posteriori errors are determined by least squares adjustment of computed baselines, and are at 68% confidence level. JRA0 is the reference point, and LUL0 is a summit point used only for adjustment.

Table 2. March 1997 Coordinates for GPS Network Points

Point		Local coordinates UTM -49 WGS84, m			Errors a posteriori σ, m		
Number	Name	East	North	Up	*dE*	*dN*	*dU*
085	DEL1	440692.1582	9163972.9435	1511.3533	0.0173	0.0095	0.0247
090	BAB0	434975.8794	9168041.2171	1321.0026	0.0158	0.0116	0.0221
100	JRA0	436180.2839	9171235.4989	1335.4256	—	—	—
105	SEL0	439543.9658	9167528.3234	2570.3769	0.0126	0.0086	0.0176
107	PUS0	439552.3021	9166838.7241	2733.9943	0.0121	0.0081	0.0160
120	LUL0	438978.0607	9166537.5390	2976.7600	0.0118	0.0078	0.0157

Same comments as Table 1.

All computed baselines (representing 42 vector components expressed in the geocentric reference frame) with a priori errors are reduced to 5-point relative positions by a least squares inversion method (3-D geodetic adjustment, J.C. Ruegg and C. Bougault, unpublished data, 1992). Then final positions of points for each period are obtained in local Universal Transverse Mercator (UTM-49) coordinates together with their uncertainties (see Tables 1 and 2). Because of the decorrelated error sources (antenna setting and atmospheric delay), the sound spatial network configuration (some baselines have a horizontal component of 3 km and a vertical component of 1.4 km), and the amount of data used for inversion, the a posteriori errors are relatively small and reflect more the redundancy of measurements than a priori errors.

Accordingly, the relative displacement vectors of the four points BAB0, DEL1, SEL0, and PUS0 are defined for the period September 1996 to March 1997 (see Table 3, Figures 8 and 9). These vectors reveal a significant global vertical downward movement with a mean value equal to –6.5 cm. Displacements of distant stations BAB0 and DEL1 are large enough to conclude that our reference point also moved. Thus these observed displacements are not absolute but relative displacements.

Table 3. Relative Displacements With Respect to JRA0 for GPS Points Between September 1996 and March 1997

Point	Relative Displacements, m			Errors σ, m		
Name	East	North	Up	*dE*	*dN*	*dU*
DEL1	+0.0266	+0.0181	–0.1252	0.0297	0.0281	0.0519
BAB0	+0.0074	+0.0176	–0.0472	0.0185	0.0140	0.0259
SEL0	+0.0039	+0.0126	–0.0636	0.0143	0.0097	0.0197
PUS0	+0.0016	+0.0107	–0.0256	0.0148	0.0102	0.0196

3. High-Precision Tilt Station

3.1. Methodology

The quality of a tilt station is defined by four characteristics, which are, in order of importance: (1) coupling of the instrument with the ground, (2) small or negligible "non-volcanic" deformation (thermal and rainfall) on the site, (3) high sensitivity and high precision of the instrument and (4) continuity and high resolution of numerical data recording. Concerning the coupling characteristics, the aim is to measure tilt variations which are representative of the motion of a large surface on the edifice. However, tiltmeters, except water tubes, measure tilt variations on a surface area which is usually less than 1 m^2. In order to extend this surface to a few tens of m^2, a solution is to install several tilt components at different locations (see Figure 3). In order to be validated, all components oriented in the same direction must give the same signal. If this is true, we know that no instrumental effects (like drift) have polluted the signals.

The second important quality of a tilt station is linked to the reduction of meteorological effects on the ground, like temperature and rainfall. This problem has been widely studied in the literature, and the best (but expensive) solution is to bury the instruments as deep as possible, as was done, for example, at Sakurajima volcano in a 290-m-deep borehole [*Ishihara*, 1990]. On the Merapi, *Minakami et al.* [1969] showed that the temperature at a depth of 1 m is almost free from diurnal variations (within a range ±1°C). Further, the flanks of Merapi are covered on a large area by a compact and massive rock identified as a 5000 years old pyroxene andesitic lava flow, with a thickness that reaches 200 m at some places [*Berthommier*, 1990]. In a few locations a few meters of young pyroclastic flows cap this rock

(see Figure 1). This soil layer constitutes an isolator as compared with the higher thermoconductive massive rock. On the interface, horizontal temperature gradient is locally almost equal to zero, and thermomechanical effects are strongly reduced by the soil layer. We chose an accessible location 3 km from the summit, on the southeast flank, for installing the tilt station and the DEL1 GPS benchmark. At this location, the soil layer thickness is equal to about 1 m, and tiltmeters have been installed directly on the basement rock (i.e., at 1 m depth).

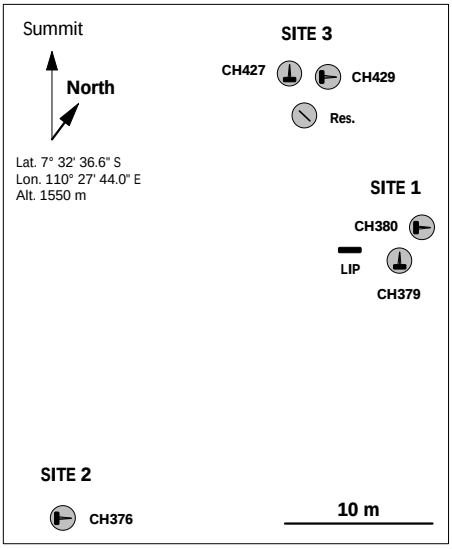

Figure 3. Schematic horizontal view of the Deles tilt station. It is located on the southeast flank (3 km from summit). The five components (three radial, CH376, CH380, CH429, and two tangential, CH379 and CH427) have been installed with three different methods. Site 1 is simply laying on a concrete, site 2 is laying directly on the lava, and site 3 is welded to the lava. LIP is a temperature sensor, and Res. a resistor bridge that simulates a virtual fixed tiltmeter.

3.2. Instrumentation

Five tiltmeters have been installed at three different sites distant from each other by about 10 m (three radial components oriented toward the summit in the N30°W direction and two tangential components, 90° anticlockwise, oriented N120°W, see Figure 3). The tiltmeters are horizontal pendulums based on the Zöllner pendulum principle, and they are made of monolithic welded silica, giving a precision of 10^{-8} rad [*Blum*, 1963; *Saleh et al.*, 1991]. Silica has a very small thermal dilatation coefficient (0.54×10^{-6} K^{-1}) and relaxation rate (-2×10^{-7} yr^{-1}), and it is not influenced by moisture and corrosion. Moreover, this principle provides a means to vary the instrument sensitivity over several orders of magnitude through the adjustment of the oscillation period of the pendulum [*Jobert*, 1959]. Each tiltmeter has its own period (from 8 to 15 s), defined during installation. This implies slightly different values of sensitivity for each tilt component (see Table 4). Thus instrumental effects, if they exist, can be identified by comparing the response of the different sensors.

Table 4. Deles Tilt Station Instrument Characteristics

Instruments	Unit	Sensitivity (mV/unit)	Digital Resolution	2-Min Noise	1-Day Noise
Tilt tan. CH379	µrad	51.698	1.15×10^{-4}	0.0121	0.4106
Tilt tan. CH427	µrad	36.646	2.00×10^{-5}	0.0117	0.7835
Tilt rad. CH376	µrad	32.263	2.14×10^{-5}	0.0136	0.3163
Tilt rad. CH380	µrad	41.071	5.40×10^{-5}	0.0099	0.3888
Tilt rad. CH429	µrad	13.846	1.00×10^{-5}	0.0302	0.2693
Rock temp. LIP	°C	100	1.75×10^{-4}	0.0050	0.0837
Resistor bridge	V	1000	1.09×10^{-3}	0.0968	0.4471

Noise is estimated by the standard deviation on signals after high-pass filtering on two important periods: 2 min for sampling period, and 1 day for daily temperature effects.

A temperature sensor has been placed within the rock, and a resistor bridge simulates the response of a stationary tiltmeter. It reflects all forms of electronic noise (acquisition, amplifiers, battery voltage, etc.). Figure 3 shows the location of each sensor. At the three sites, sensors are protected by a steel box covered by a 5-cm-thick isolator. These boxes are then buried under a 1-m cover of natural soil.

For a perfect recording continuity, two data loggers are used (micro Data Acquisition System (µDAS), 20-bit and four-channel continuous integrators) [*Van Ruymbeke et al.*, 1997] instead of radio-transmitter systems. On each sensor, voltages are converted to frequency modulated signals in order to suppress long cable effects. The µDAS directly records frequency of the signal by a simple counter. Thus the recording system constitutes a perfectly linear integrator, with very high-range digital conversion [*Beauducel*, 1991]. Each data logger has its own power supply system (solar panel and batteries), and there is no possibility of electronic interaction between them. For a 120-s sample (and integration) period, autonomy is more than 2 months before data downloading. Table 4 gives the values of sensitivity, digital resolution, and noise for each instrument. It shows the relatively high precision of tilt measurement and the limited temperature effects (mean standard deviation of 0.43 µrad on daily variations). By comparison, diurnal tilts at Mount St. Helens were 50 to 200 µrad for typical surface installation and a few microradians for an instrument buried 1 m deep in an artificial vault [*Dzurisin*, 1992].

On Merapi, Deles station was installed in September 1995, and after various technical problems, it has been operational nonstop since July 1996. However, one radial component (CH380) had to be reinstalled in November 1996 and was still drifting during the period considered here, i.e., November 1996 to March 1997.

3.3. Results

Because of the small but obvious correlation of tilts with ground temperature, each signal has been corrected with a nonstationary linear method (described in the Appendix). This improves the global signal-to-noise ratio by about 10%. Figure 4 shows the relative tilt signals of the station in both directions (two radial and two tangential), for the period bounded by the two GPS campaigns. Figure 4 confirms that the two tangential and the two radial sensors record identical long-term signals and are free of any instrumental effects. The complete independence

of components provides a means to measure the real tilting of a 30 m × 10 m area at the site and, more importantly, to estimate an error on the tilt measurement. Short-term variations (with periods less than a week) are not consistent within a range of ± 1 µrad. This suggests that site effects on tilts are less than this value. No significant signal is observed at the date of eruption.

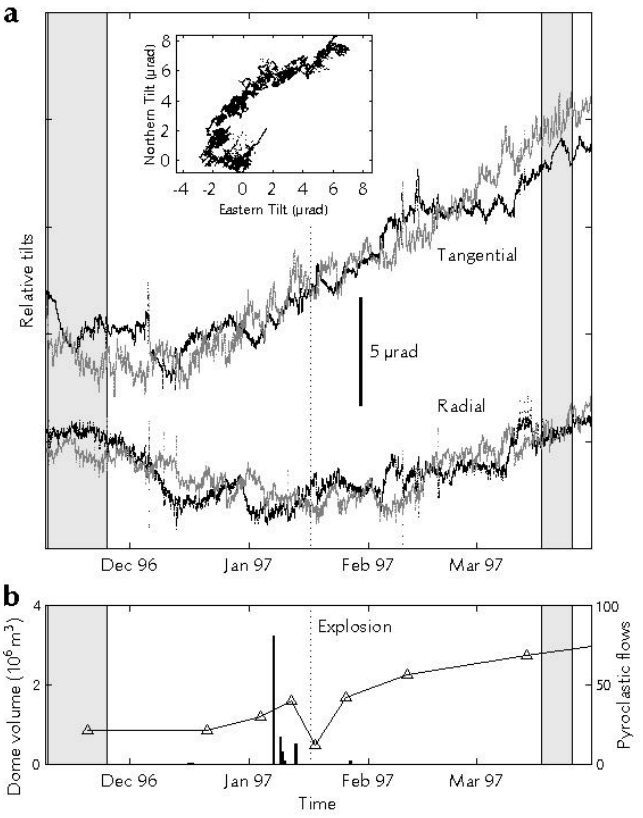

Figure 4. (a) Relative tilt signals at Deles station for two components in the tangential direction (CH379 and CH427) and two components in the radial direction (CH376 and CH429). Each signal is corrected from temperature effects by a non-stationary linear method. Inset plot shows the horizontal projection of the motion of the tip of the normal to ground surface (radial versus tangential average signal). *(b)* Dome volume estimation (solid line and triangles) and number of pyroclastic flows (bars) within the period. Shaded zones represent GPS campaign periods. Dotted vertical line corresponds to the time of explosion (January 17, 1997, 1034 LT).

The observed tangential (11.1 ± 0.7 µrad) and radial (0.9 ± 0.4 µrad) averaged tilts and standard deviations indicate a global tilting on site of 11.1 ± 0.4 µrad in the N60°E ± 2° direction. The tilt varies continuously in time but not linearly, as is shown by the inset plot in Figure 4.

4. 3-D Elastic Modeling

The first objective of modeling is to locate the deflation (or inflation) source and to determine the associated magma volume variation that fits the data best. Data consist of four relative displacements (4 times three components) and one tilt variation (2 components), i.e., only 14 data. Given the values of observed tilts and displacements and given the anticipated geometry, location, and loading conditions of the source, an elastic solution has been searched for. As is shown by *Dvorak and Dzurisin* [1997], elastic modeling on active volcanoes for describing surface displacements has been validated in many cases.

4.1. Forward Problem: Topography Effects

4.1.1. Importance of a 3-D model. Mount Merapi, with its 2964-m altitude and its average slopes of 30° (which reach 57° near the summit), exhibits a real three-dimensional topography. Significant errors on source depth and volume variation estimations are made when using a half space model for interpreting surface deformation on prominent volcanoes [*McTigue and Stein*, 1984; *McTigue and Segall*, 1988; *Cayol and Cornet*, 1998a,b]. Moreover, the asymmetry of the northeast flank and the closeness of Mount Merbabu (3142 m) to the north side prohibit any axisymmetrical approximation. Accordingly, the 3-D mixed boundary elements approach (MBEM) [*Cayol and Cornet*, 1997] has been adopted for the forward problem computation. It takes into account 3-D topography for the ground surface and magma reservoirs with complex geometry. The loading imposed by the magma chamber is modeled by a small pressure variation acting on the chamber surface. This pressure variation induces a change in chamber volume. The relation between surface displacement and changes in chamber volume are independent of the Young modulus of the medium. Since we are looking for magma chamber volume variation and not pressure, we avoid the difficult task of estimating this elastic parameter.

4.1.2. Mesh of the ground surface. A Digital Elevation Model (DEM) of the Merapi region computed from two SPOT images taken in 1987 has been used. The original DEM contains large areas where data are missing because of clouds on eastern portions of Merapi and Merbabu. These have been corrected by considering several topography points, which have been interpolated [*Jousset*, 1996]. Also, detailed analysis of this DEM has revealed, locally, errors in the order of a few hundred meters on the flank of some valleys, because of oblique sunlight when the images were taken. This is particularly noticeable in the vicinity of the tilt station. These errors may result in false computation for tilt direction and amplitude. Consequently, this area has been replaced by a more accurate digitized topography map [*U.S. Army*, 1964]. Moreover, this detailed map helped to locate the tilt station very precisely (± 10 m), i.e., within an error consistent with the spatial resolution on tilt data. The surface is meshed by a series of imbricated square grids centered on the tilt station location. The point density of the mesh decreases while going away from the center area. Elements are constituted by triangles of the Delaunay type, and the smallest are 20 m large (see Figure 5a) .

The validity of this mesh was controlled a posteriori by examining the results obtained with the final source model (see section 4.4 below). Figure 5b shows the relative tilt variations along 500-m-long cross sections oriented both in radial and tangential directions. It is seen that tilting is very dependent on topography but does not exceed 1 µrad on adjacent elements at the Deles tilt station. Our mesh gridding is consistent with this result.

4.1.3. Shallow magma chamber. A first magma chamber model at Merapi has been proposed after the observation of an aseismic domain located between 1 and 3 km below the summit [*Ratdomopurbo*, 1995; *Ratdomopurbo and Poupinet*, 1995]. Volume and conduit length inferred from this reservoir geometry are consistent with the magma flux associated with the lava dome extrusion of the 1994 eruption and the gravity changes observed between 1993 and 1994 [*Jousset et al.*, 1998].

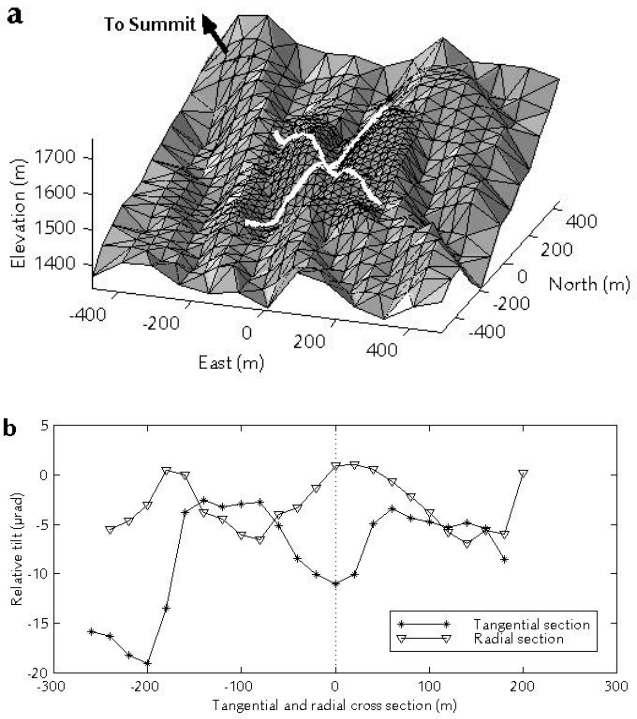

Figure 5. (a) Three-dimensional (3-D) mesh of topography around the Deles tilt station derived from a digitized *U.S. Army* [1964] map. Elements are Delaunay type, and the smallest are 20 m wide. The two white lines represent radial (summit direction) and tangential cross sections. Zero distance coincides with the tilt station. (b) Relative tilts computed along the cross sections for the final source solution. In 20 m, variations are less than 1 μrad.

We conducted a first calculation on the basis of this model, with a spherical chamber with radius r = 850 m centered at depth z = 1000 m (above sea level). Displacements and tilts associated with an arbitrary volume variation $\Delta V = 1\times10^6$ m^3 are shown in Figures 6 and 7. The results of this first calculation are as follows: (1) displacement amplitudes are almost centered on the summit and unperturbed by topography. In this model, the GPS reference point is far enough from the maximum displacement so that it may be considered as a real static point. (2) Tilt amplitudes are less than 10 μrad, 3 km away from the summit. (3) Topographic effects on tangential displacement (which are very small) and tilt are clearly seen, although they are equal to zero for *Mogi*'s [1958] model. Maximum tilt is located on the southeast flank 1.5 km away from the summit. It was also found that near the tilt station, topography effects induce differences up to 300% of amplitude in tilt and 180° in direction as compared to the simplified half-space model.

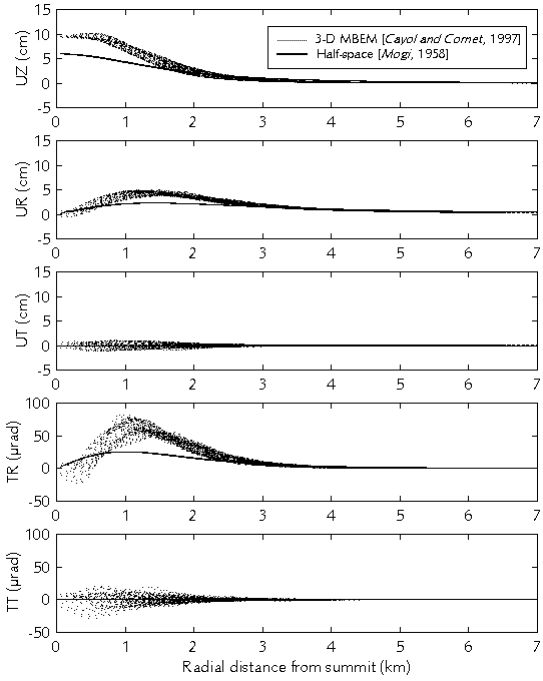

Figure 6. Surface displacements and tilts associated with a one-million m^3 inflation in a spherical magma chamber located below the summit (aseismic zone). Each point represents a location on the meshed surface. Data are presented in a cylindrical referential centered at Merapi summit. Solid lines show the same parameters for the half-space solution. The 3-D topography effects are clearly observed especially on tangential displacement and tilt. UZ, vertical, UR, radial, and UT, tangential displacement; TR, radial, and TT, tangential tilt.

In order to improve the consistency of this model with the data, we adjusted the only parameter of the model (volume variation) since it has a linear effect on displacements. We obtained a very poor misfit value equal to 110 (see Table 5 and equation (4) for the definition of misfit). Accordingly, we decided to look for a new location for the magma source following an inverse problem method.

4.2. Inverse Problem Method

The inversion method consists of the search for some of the model characteristics by relying only on the forward problem formulation and on the observed data. Here the model is reduced to a set of chosen parameters vector $\mathbf{m} = \{m^1, m^2,...\} \in \mathbf{M}$, where $\mathbf{M}$ is the "model space". For a given model $\mathbf{m}$ the function which measures the degree of misfit between observed data $\mathbf{d_{obs}} = \{d^1_{obs}, d^2_{obs},...\}$ with errors $\boldsymbol{\sigma}_{\mathbf{obs}} = \{\sigma^1_{obs}, \sigma^2_{obs},...\}$, and the values predicted with the model $\mathbf{d_{cal}} = \{d^1_{cal}, d^2_{cal},...\}$, is called the "misfit function" $S(\mathbf{m})$.

If the forward problem is solved by the equation

$$\mathbf{d}_{cal} = \mathbf{g}(\mathbf{m}) , \qquad (3)$$

then the misfit function for N data with Gaussian experimental uncertainties is given by

$$S(\mathbf{m}) = \tfrac{1}{2}\sum_{i=1}^{N}\left(\frac{d^i_{\text{cal}} - d^i_{\text{obs}}}{s^i_{\text{obs}}}\right)^2, \quad (4)$$

which presents a minimum for the best parameter set **m**. The "likelihood" function $L(\mathbf{m})$ is defined as the a posteriori probability of a model:

$$L(\mathbf{m}) = k\exp\left[-S(\mathbf{m})\right]. \quad (5)$$

This function helps to define the best parameter set **m** (expected maximum value) and the "quality" of the solution (standard deviation for each parameter σ_{cal}).

The relatively long time required for computing the forward problem solution with the MBEM (about 1 hour on a Sun Sparc Ultra 1 station, 96 Mbyte RAM) preempts an "exhaustive search" method for finding the parameter values. The gradient method cannot be applied here because of the non linearity of the misfit function. Thus we opted for a slightly modified Monte Carlo near-neighbor sampling method [*Tarantola*, 1987]. Starting with a current model $\mathbf{m}_{\text{current}}$ with an associated coefficient equal to 1 (called "weight" in this paper), a new "trial model" is chosen pseudorandomly within a neighborhood of parameters $\mathbf{N} \subset \mathbf{M}$. If the condition

$$S(\mathbf{m}_{\text{trial}}) < S(\mathbf{m}_{\text{current}}) \quad (6)$$

is satisfied, the trial model becomes the new current model. If not, the current model is kept, but its weight is increased by 1. The parameter intervals that characterize the space **N** are arbitrarily chosen. These interval values influence the speed of convergence but not the final solution. The collection of current models $\mathbf{m}_1$, $\mathbf{m}_2$,... and their associated misfit values are a representative sample of **M**. The process can be stopped by a condition on the current model weight, for instance, reaching a chosen value. The last current model (with maximum weight) is the best one.

Because in an elastic volcanic structure, displacements are proportional to the magma chamber volume variation, the inversion process can be accelerated in the following manner. Instead of choosing a random value at each trial model for the volume variation, this parameter is fixed to unity and adjusted a posteriori with a coefficient that minimizes the misfit function. This inversion method needs a priori values for the parameters for initializing the iterative process. In order to fix the first current model not too far from the final solution, we consider the elastic infinite half-space analytical solution, which allows a fast inversion (computation time of the forward problem becomes sufficiently low to explore thousands of models).

4.3. First Model: Spherical Source

Surface displacements associated with a point dilatation in an elastic semiinfinite space have been described by *Anderson* [1936]. This solution has been widely used in the literature for modeling magma chamber as spherical source approximation [*Mogi*, 1958], when the mean radius of the chamber is much smaller than the depth of it ($a << d$, where a is the cavity radius and d is the depth). *McTigue* [1987] showed that first-order correction for a finite spherical magma body varies like ε^6, where $\varepsilon = a/d$, and reaches only 10% for $\varepsilon = 0.5$. This implies that a point source is a very satisfactory approximation and that the size of the sphere has not much significance on surface deformations.

Mogi's [1958] model involves four parameters (depth and horizontal coordinates of source and change in volume). In our case, we have to take into account relative displacements; that is, we must determine the four parameters.

A four-parameter model space has been explored: source position (X, Y, Z) and volume variation ΔV. The best model corresponds to a deflation source of 24×10^6 m^3, located 6 km deep, 4-km eastward from the summit (see Table 5). Each parameter can be associated with a standard deviation estimated from the probability function $L(\mathbf{m})$. The three components of SEL0 and PUS0 and the two components of tilt are correctly reproduced (error lower than 1 σ). On the contrary, vertical component of BAB0 and horizontal orientation of DEL1 displacements are not satisfactory. Considering that this misfit is due to an effect resulting from the half-space simplification, we used this solution as first model for the inverse problem with topography.

For this inversion the source is a real sphere with a 1200-m radius. It corresponds to a volume of 7.2×10^9 m^3 that has been chosen so as to fit the ratio determined by *Blake* [1981], i.e., about 3 orders of magnitude larger than the erupted magma volume. Two hundred and sixty-three forward problems have been computed with a last current model weight equal to 21. The best model is a deflation source of 11×10^6 m^3 located 3.7 km below the summit and 2 km to the east of it. This confirms the results of *Cayol and Cornet* [1998a] that for a 30° slope volcano, *Mogi*'s [1958] model overestimates the volume variation as well as the depth of the source (referred with respect to the summit elevation) by as much as 50%. Horizontal location is slightly different from the half-space solution, and it is closer to the summit because of the important topographic effects on tilt. However, the misfit function is still high, and the topography does not explain the DEL1 horizontal displacement. Surprisingly, the value of the misfit is worse when taking into account the topography (5.9 instead of 5.1, see Table 5). In order to try to improve the fit to the data, an ellipsoidal shape has been considered for the source.

4.4. Second Model: Ellipsoidal Source

In order to determine the a priori model required for initializing the inversion process, we ran a preliminary inversion corresponding to an ellipsoidal source in an elastic infinite half-space. Because of its simplicity, the solution for a fault in purely opening mode [*Okada*, 1985] has been chosen for characterizing the ellipsoidal source. Indeed, surface deformations associated with a mode 1 fault discontinuity are very similar to those observed with an ellipsoidal source, except for shallow depth where fault tip effects become significant. We associate the opening mode with a volume increase so that a deflation is modeled by a negative displacement discontinuity. The dislocation is assumed to be square with a fixed dip angle, which reduces the number of parameters of *Okada's* [1985] model to 6.

4.4.1 Vertical sheet. From the same 14 data as in the first model, we explored a six-parameter model space defined by the

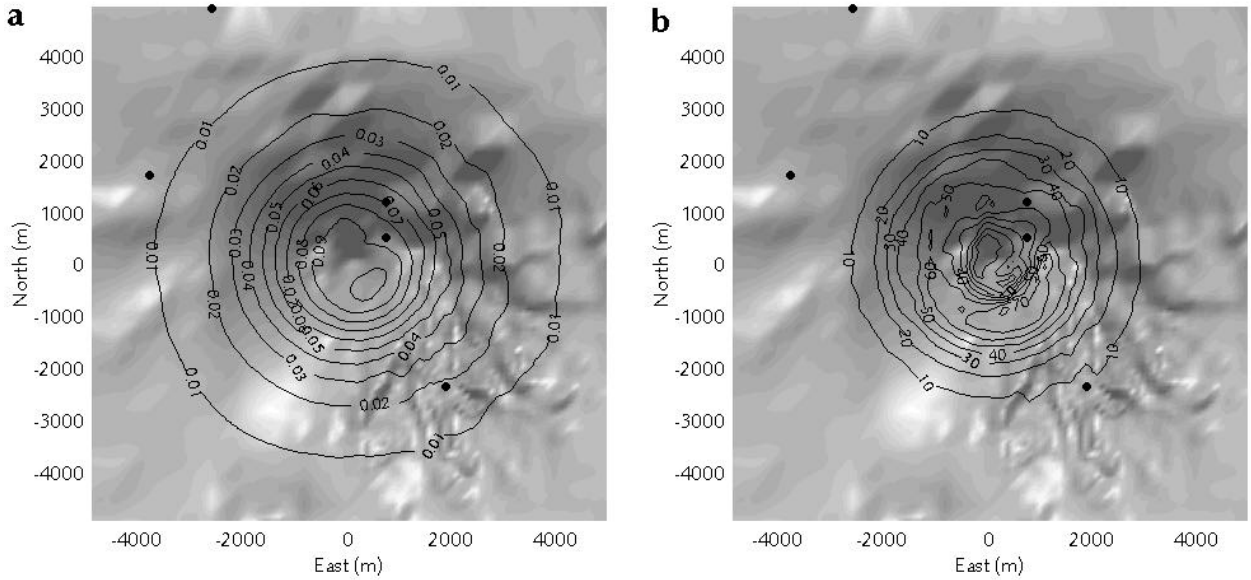

Figure 7. (a) Displacement relative amplitudes and (b) tilt amplitudes associated with a one-million m^3 inflation in a spherical magma chamber located below the summit, showing the horizontal view in coutour lines of isovalue over lighted topography (see also Figure 6). Black dots correspond to GPS benchmarks location.

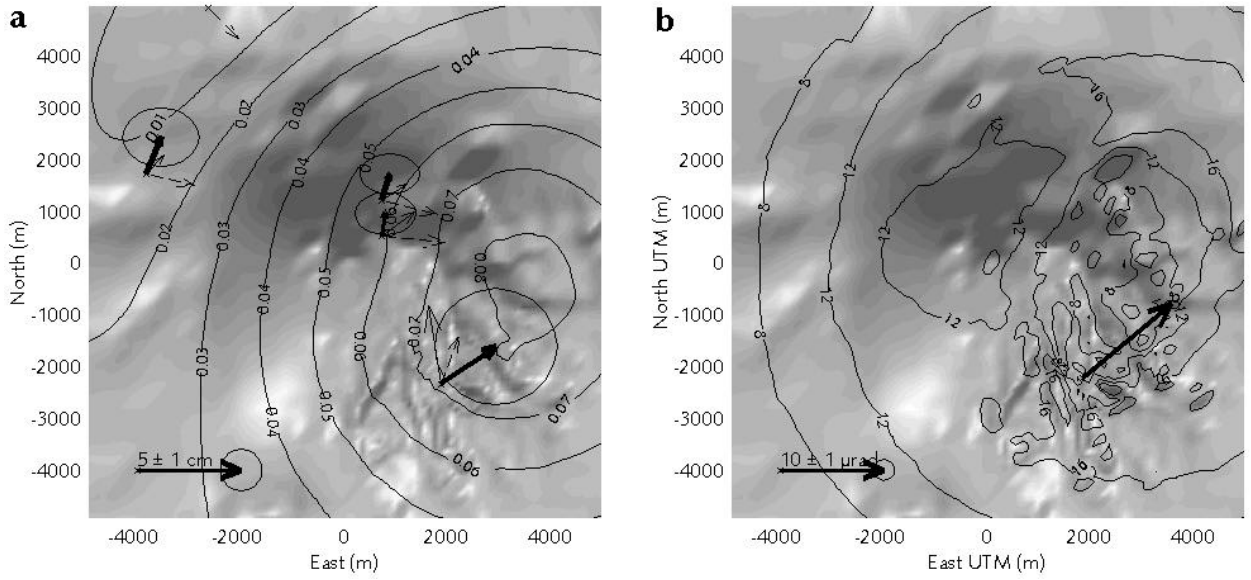

Figure 8. Horizontal projection of (a) GPS displacements and (b) tilt data (heavy solid line) with 1-σ ellipsoidic confidence errors and final model solution. In Figure 8a, light solid lines stand for the model relative displacements, and ashed lines stand for the model absolute displacements. Level curves show relative displacement and tilt amplitudes computed by the model. Local effects on tilts are obvious.

position of the center point of the upper edge of the sheet (*X*, *Y*, *Z*), the side length *L*, the horizontal orientation (strike) *S*, and the volume variation Δ*V*. Only tilt is correctly adjusted with the opening of a vertical 8-km-deep, 3-km sided square sheet (see Table 5). Displacements are very poorly fitted, and we observed in the various models that displacements and tilts cannot be fitted simultaneously by a single model. Since tilt data are better constrained (relative errors smaller than for displacements), the solution fits the tilt data but not the displacements. It is concluded that data are incompatible with a vertical fault source; that is, if the source has a preferential orientation, it is not in the vertical direction.

Table 5. Solutions Found for Different Models of Magma Source

Source	Source Inversion Parameters					Misfit
	X, km	*Y*, km	*Z*, km	*S*, deg	ΔV, 10^6 m^3	S_{min}
Sphere [a]	0.0 [b]	0.0 [b]	–1.9 [b]	—	–0.47 ± 0.03	110
Point [c]	4.4 ± 0.1	–0.4 ± 0.2	–9.0 ± 0.1	—	–23.6 ± 1.4	5.1
Sphere [a]	2.0 ± 0.3	0.0 ± 0.2	–6.6 ± 0.2	—	–11.0 ± 1	5.9
Vertical fault [d]	2.7 ± 1.1	–1.6 ± 1.4	–10.0 ± 1.4	–48 ± 12	(+101 ± 66)	8.5
Horizontal fault [d]	2.8 ± 1.0	–0.9 ± 1.4	–11.9 ± 1.6	—	(–24.3 ± 13)	4.9
Horizontal ellipsoid [d]	2.2 ± 0.4	–0.1 ± 0.4	–8.7 ± 0.4	—	–10.8 ± 2.2	5.3

(*X*,*Y*,*Z*) are east, north and up positions with respect to the summit, *S* is the strike (for vertical fault model), and ΔV is the volume variation. Each parameter is given with its standard deviation estimated from the a posteriori probability function of the model space. For elastic half-space models [*Mogi*, 1958; *Okada*, 1985] the virtual horizontal ground surface has been defined at the GPS reference point JRA0 elevation (1330 m). Fault modeling refers to a mode I dislocation (opening mode only).

[a] MBEM [*Cayol and Cornet*, 1997].

[b] Fixed values.

[c] *Mogi* [1958].

[d] *Okada* [1985].

4.4.2. Horizontal sheet. With the same parameters the best model yields a fault in deflation, 2.3 km wide and 9 km deep, with a better misfit value than any of the previous models (see Table 5). This solution was used as a first-trial model for the inverse problem with topography.

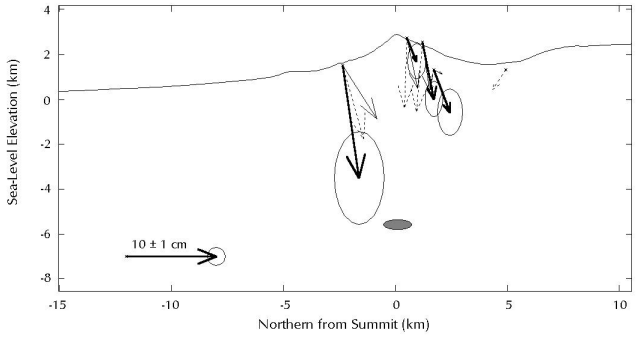

Figure 9. South-north vertical projection of GPS displacements and final solution displacements (same comment as Figure 8).

4.4.3. Final solution. For the ellipsoidal source, three solutions with different volumes for the chamber were computed: same volume as that for the spherical source ($a = b = 1731$ m for horizontal axis and $c = 577$ m for vertical axis) and then volumes 8 times and 27 times smaller than that of the sphere. Two hundred and three forward problems were computed with a last current model weight of 72. The best model is a deflation source with a decrease in volume equal to $10.8 \pm 2.2 \times 10^6$ m^3, located 5.8 ± 0.4 km deep and 2 ± 0.4 km east from the summit. The minimum misfit value equals 5.3. It is higher than that for the half-space model but better than that for the spherical model with topography (see Table 5). There is no significant difference (source position and volume variation) between the solutions obtained with the three chamber volumes. It is concluded that this modeling cannot resolve the initial source volume. Figures 8 and 9 show the computed displacements and tilt vectors as compared to the data. As for previous models, vertical displacement of BAB0, horizontal direction, and vertical displacement of DEL1 are not reproduced satisfactorily. Figure 10 shows the model space samples for the sphere and for the ellipsoid sources, as a function of volume variation versus depth. It reveals the linear dependency between these two parameters (the shallower the depth, the lower the volume variation) and the independency of the volume variation with respect to source shape and size.

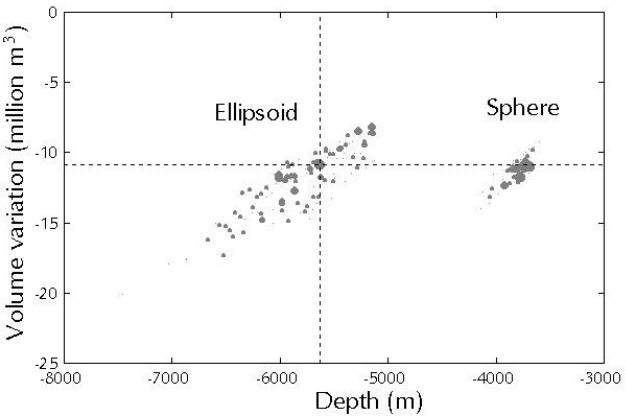

Figure 10. Model spaces for ellipsoidal and spherical sources, as a function of volume variation versus depth. Dot size stands for probability of each model. A positive correlation appears for both models. The source geometry affects only the depth not the volume variation.

5. Discussion

5.1. Methodology

5.1.1. Tilt modeling. All the tested models adjust exactly the two tilt data, because of the relatively small uncertainty associated with their measurement as compared to that on displacements. These tilt data have an important part on the inversion because they fix the horizontal position of the source; thus they eliminate a set of models which would have been selected had only displacement data been considered. However, we know that tilting is dependent of local surface topography. This entails three conditions if tilts are to be introduced efficiently in modeling: (1)

Tilt data have to be correctly measured and validated in order to represent the real tilting of the sites with large enough area. (2) It is essential to determine the realistic error associated with the measurement, because the inverse problem solution is highly constrained by data uncertainties. (3) Three-dimensional topography has to be accurately digitized and meshed in order to be used in the model.

5.1.2. Model Validity. We were not able to fit our complete data set but only 11 out of the 14 data for a four-parameter model. Nevertheless, this result provides a significant appreciation of the source position and its volume variation. The Monte Carlo inversion method which has been used allows us to determine probabilistic errors (one standard deviation) for each parameter estimation. These errors are equal to few hundred meters for source position and 2.2×10^6 m^3 for volume variation. These errors stand only for the final solution, i.e., for a fixed source size. We showed that the source depth is dependent with the chamber shape and that volume variation is independent with the chamber size. With the presently limited database it has not been possible to constrain the size of the chamber, but we clearly showed that a vertical shape is improbable. This suggests that below the Merapi at few kilometers depth, the vertical stress component is the minimum principal stress component, a feature consistent with the regional tectonics.

5.2. Volcanological Aspects

The position of the source which has been found is not incompatible with the existence of a shallow magma chamber as proposed by *Ratdomopurbo* [1995]. Indeed, the periods of study are not the same, and it may be supposed that the two magma reservoirs exist. Our data reveal that the deeper chamber had a prominent activity during this eruption period and that if it exists, the upper chamber did not sustain any variation in pressure.

The volume variation found by our model ($-10.8 \pm 2.2\times10^6$ m^3) can be compared with the estimated volume of produced lava at the summit. If we suppose that all the deflation volume has been extruded at the summit, only 30% (3.2×10^6 m^3) of it corresponds to the dome formation. The remainder (7.6×10^6 m^3) cannot have been ejected instantaneously from the deep reservoir during the explosion because the continuous tilt records show that the deflation of the source was regular (see inset in Figure 4) during the 5-month period. Also, the magma cannot have accumulated in a temporary shallow location during the period preceding the explosion. Indeed, a volume variation of this magnitude would have induced a tilt amplitude equal to about 80 μrad at the Deles station (see section 4.1). Given the tilt signals, the volume variation in the deep magma chamber must correspond exactly to the volume of lava produced at the summit. This difference between calculated and observed volumes (a factor 3) leads to two consequences:

1. On the basis of our model and because the model uncertainty has been well determined, we conclude that the volume of extruded lava has not been estimated correctly. The missing $7.6 \pm 2.2\times10^6$ m^3 corresponds very likely to the volume of continuous rock avalanches, which occurred during this period. A simple calculation shows that the missing volume can be included in a quadrangular prism 2 km long, 2 km wide at the bottom, 300 m wide at its top (crater) and 5.3 ± 1.5 m thick near the crater, with no thickness at the bottom.

2. The explosion did not involve large magma volumes and was only superficial.

6. Conclusion

Deformation measurements obtained for the period November 1996 to March 1997, provide some constraints on the magma chamber at the Merapi volcano. Taking into account a 3-D topography and including both displacements and tilt observations in an inversion process modifies the conclusions of the classical half-space modeling approach and, hopefully, yields results closer to reality.

We determined that for the period of concern and despite a strong explosion, the deformations were almost continuous in time and are due to a deflation of a deep magma source located some 6 km below sea level. The corresponding magma production can be related only partly to the surface dome growth and suggests that the volume of rock avalanches is equal to about 3 times the volume of the dome growth as detected at the crater level.

This type of study has been possible because (1) a noninterrupted data set for the complete duration of the selected eruption period was available, (2) realistic uncertainties have been determined for each type of data, and (3) a digital elevation model with a spatial precision consistent with the data was available. This limited data set helps only to improve slightly the comprehension of Merapi behavior. However, this methodology should prove efficient for determining precisely the shape and the depth of the magma chamber when more data are available.

Appendix: Temperature Correction of Tilt Signals

Sensitive surface deformation measurements are challenged with a major problem: even if the instrument is exempt from temperature effects, it measures real ground deformation due to meteorological parameters like temperature and rainfall. Attempts to model these effects have shown that the relation-ship between temperature and tilt is usually linear to the first order but variable in time and different for each frequency [*Berger*, 1975; *Goulty et al.*, 1979; *Mortensen and Hopkins*, 1987; *Desroches*, 1990; *Beauducel*, 1992]. With rainfall the relation-ship is strongly nonlinear if the water table level is at shallow depth [*Wolfe et al.*, 1981; *Evans and Wyatt*, 1984]. On Merapi the water table is about 1000 m below the Deles tilt station (H. Shibano et al., unpublished data, 1994); thus the ground is almost always unsaturated, even a few hours after a hard rainfall.

If $S_{obs}(t)$ is the observed signal (measured tilt) and $N(t)$ is the disturbing signal (measured temperature), then the problem of identifying tilt associated with sources other than temperature can be expressed by

$$S_{obs}(t) = S(t) + G[N(t - \tau)] , \qquad (7)$$

where $S(t)$ is the tilt free of temperature effects and G is an unknown function.

This problem comes down to estimating G from $S_{obs}(t)$ and $N(t)$. This cannot be resolved without some a priori information on unknown parameters of equation (7), and the danger is to include characteristics of $S(t)$ into the function G. Classical autoregressive methods (like the Wiener filter) suppose that $S(t)$ is a random or a "white" signal [*Kofman et al.*, 1982], but we know that this is not the case with tilt on volcanoes.

A simple method is proposed here for removing most temperature effects from a tilt signal. This method does not imply strong hypothesis on $S(t)$ but relies strongly on the hypothesis that G is a linear function of N. Furthermore, every step of the signal processing is performed in the time domain, in order to avoid introducing numerical noise by the time-frequency domain transform. For instance, high-pass filtering with cut-off period p is based on zero-phase moving average (ZMA) [*Oppenheim and Schafer*, 1989] defined as

$$F_p\{s(t)\} = s(t) - ZMA_p\{s(t)\} \; . \tag{8}$$

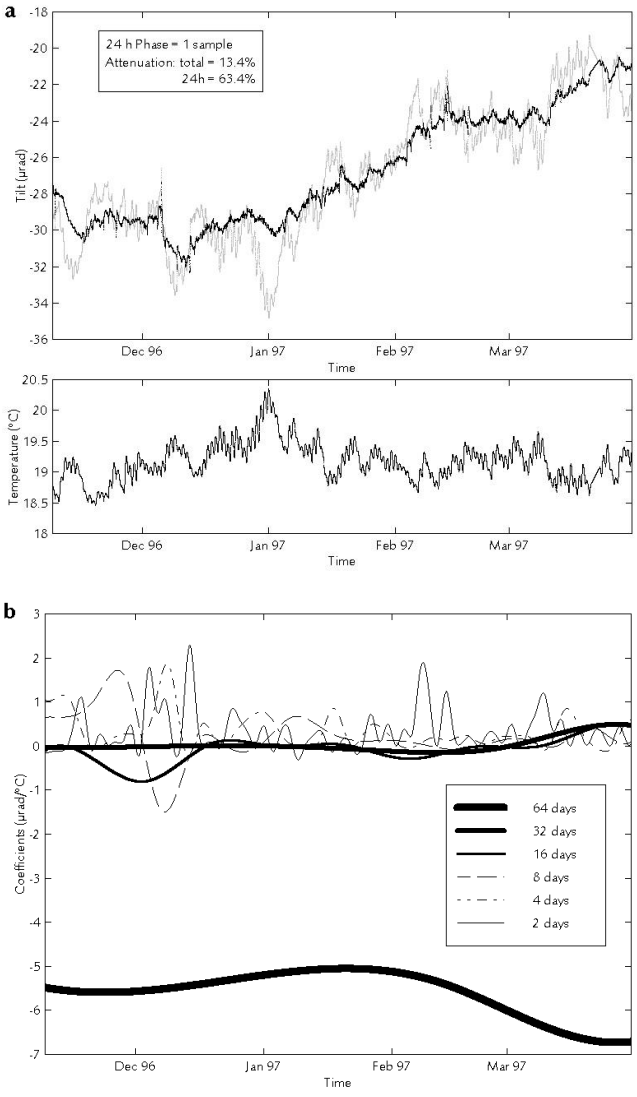

Figure A1. Example of temperature correction on tilt signal (CH379, tangential) for (a) original tilt (dotted lines) and final corrected tilt (solid lines), following temperature and (b) linear evolutive functions $C_p(t)$ for each p values.

We first determine the phase lag τ between the two signals, determined by cross correlation on $F_{day}\{S_{obs}(t)\}$ and $F_{day}\{N(t)\}$. Let us consider a time interval T defined between $t - p/2$ and $t + p/2$. For each value of t we compute the linear correlation coefficients from covariance matrix between $X = F_p\{S_{obs}(T)\}$ and $Y = F_p\{N(T - t)\}$. Let us define the fitting coefficient as $r_p(t) = (C_{XX}\, C_{YY})^{-½}$, variying between 0 for uncorrelated signals and 1 for perfect correlation, and $c_p(t) = C_{XY}/r_p(t)$ as the slope. Then we compute a continuous function $C_p(t) = c_p(t)\, r_p(t)$, which represents the evolutive linear coefficient for all periods lower than p. In this example, $C_p(t)$ is expressed in µrad.°C^{-1}. Note that the use of coefficient $r_p(t)$ as a factor suppresses the possibility of artifacts. Correction for period p is given by

$$S_p(t) = S_{obs}(t) - C_p(t)\, F_p\{N(t - \tau)\} \; . \tag{9}$$

This process is iteratively repeated with different values for p. For each step, p decreases by a factor 2. It is realistic to limit the maximum period to the third of the total time interval. Figure A1 presents an example of original and corrected tilt signal, temperature, and the set of correlation functions $C_p(t)$ for p = {64, 32, 16, 8, 4, 2} days, for a total interval of 142 days. It is obvious that for each period the correlation is nonstationary. Global noise attenuation is about 13% and reaches 63% for daily variations.

Some residues clearly remain in the corrected signal (especially for the 1-week period), but the correlation with temperature is not linear and strongly phase-shifted. Decorrelation of these residues cannot be done without an a priori on the second-order characteristics of function G.

In conclusion, the method is not optimal for a global noise reduction, but it respects short-period events like steps in tilt signal. The process was applied to another period in May 1997, which is much more quiet (no volcanic effects); the residue shows clearly diurnal and semidiurnal tidal waves, consistent in amplitude and phase with theoretical tilt tides [*Beauducel*, 1998]. This method is presently used with success at Montagne Pelée observatory [*Viodé*, 1997].

Acknowledgments. This work was supported by Délégation aux Risques Majeurs (French Department of Environment) and Volcanological Survey of Indonesia in the framework of the French-Indonesian Cooperation in Volcanology. We are very grateful to G. Poupinet, W.S. Tjetjep, R. Sukhyar, M.A. Purbawinata and Surono for their continuous support. For great help on tilt station installation, maintenance, and their participation in GPS campaigns, we thank the Merapi Volcano Observatory team, E. Suhanto, Saleh, Herry, C. Courteille, P. Jousset, and the CSN's from French Embassy in Jakarta : M. Dejean and J. Guilbert, successively. M. Kasser and T. Duquesnoy have initiated the GPS network measurement in 1993 and 1994. Thanks to P.A. Blum and M.F. Esnoult for constructing the tiltmeters, and to Y. Okada for providing us with his FORTRAN routines. Many thanks to the reviewers P. Segall and P. Delanay for constructive comments.

References

Allard, P., D. Carbonnelle, D. Dajlevic, N. Metrich, and J.C. Sabroux, The volatile source and magma degassing budget of Merapi volcano: Evidence from high-temperature gas emissions and crystal melt

inclusions, paper presented at Merapi Volcano Decade International Workshop, UNESCO-VSI, Yogyakarta, Oct. 1995.
Anderson, E.M., Dynamics of the formation of cone-sheets, ring-dikes, and cauldron-subsidences, *Proc. R. Soc. Edinburgh*, *56*, 128-157, 1936.
Baby, H.B., P. Golé, and J. Lavergnat, A model for the tropospheric excess path length of radio waves from surface meteorological measurements, *Radio Sci.*, *23*, 1023-1038, 1988.
Beauducel, F., Chaîne de contrôle et d'acquisition pour instruments géodynamiques, report, 75 pp.,ORB-ECAM, Brussels, 1991.
Beauducel, F., Modélisation d'une crise intrusive au Piton de la Fournaise: Atténutation des perturbations thermomécaniques sur les mesures de déformations, in *Rapports de Stage DEA*, *1*, pp. 47-81, Inst. de Phys. du Globe de Paris, France, 1992.
Beauducel, F., Structures mechanical behaviour of Merapi volcano, Java: A methodological approach of the deformation field (in French), Thèse de Doctorat, 260 pp., Univ. Denis Diderot Paris VII, Paris, 1998.
Berger, J., A note on thermoelastic strains and tilts, *J. Geophys. Res.*, *80*, 274-277, 1975.
Berthommier, P.C., Etude volcanologique du Merapi: téphro-stratigraphie et chronologie - produits éruptifs, *Thèse de Doctorat*, 180 pp., Univ. Blaise Pascal, Clermont-Ferrand II, Clermont-Ferrand, 1990.
Blake, S., Volcanism and the dynamics of open magma chambers, *Nature*, *289*, 783-785, 1981.
Blum, P.A., Contribution à l'étude des variations de la verticale en un lieu, *Ann. Geophys.*, *19*, 215-243, 1963.
Botton, S., F. Duquenne, Y. Egels, M. Even, and P. Willis, *GPS localisation et navigation*, Editions Hermès, Paris, 1997.
Cayol, V., and F.H. Cornet, 3D mixed boundary elements for elastostatic deformation field analysis, *Int. J. Rock Mech. Min. Sci.*, *34*, 275-287, 1997.
Cayol, V., and F.H. Cornet, Topography and the interpretation of the deformation field of volcanoes, *Geophys. Res. Lett.*, *25*, 1979-1982, 1998a.
Cayol, V., and F.H. Cornet, 3D modeling of the 1983-1984 dike intrusion at Piton de la Fournaise volcano, Réunion Island, Indian Ocean, *J. Geophys. Res.*, *103*, 18025-18038, 1998b.
Desroches, J., L'inclinométrie: Une méthode de suivi des opérations hydrauliques dans un milieu naturellement fracturé ?, Thèse de Doctorat, 250 pp., Univ. Denis Diderot Paris VII, Paris, 1990.
Dixon, T.H., An introduction to the Global Positioning System and some geological applications, *Rev. Geophys.*, *29*, 249-276, 1991.
Dvorak, J.J., and D. Dzurisin, Volcano geodesy: The search for magma reservoirs and the formation of eruptive vents, *Rev. Geophys.*, *35*, 343-384, 1997.
Dzurisin, D., Electronic tiltmeters for volcano monitoring: Lessons from Mount St. Helens, in *Monitoring volcanoes: Techniques and strategies used by the staff of the Cascades Volcano Observatory, 1980–90*, *U.S. Geol. Surv. Bull.*, *1966*, 69-83, 1992.
Evans, K., and F. Wyatt, Water table effects on the measurements of Earth strain, *Tectonophysics*, *108*, 323-337, 1984.
Goulty, N.R., P.M. Davis, R. Gilman, and N. Motta, Meteorological noise in wire strainmeter data from Parkfield, California, *Bull. Seismol. Soc. Am.*, *69*, 1983-1988, 1979.
Gurtner, W., G. Beutler, S. Botton, M. Rothacher, A. Geiger, H.G. Kahle, and D. Schneider, The use of the Global Positioning System in mountaineous areas, *Manuscr. Geod.*, *14*, 53-60, 1989.
Hopfield, H.S., Tropospheric effect on electromagnetically measured range: Prediction from surface weather data, *Radio Sci.*, *6*, 357-367, 1971.
Ishihara, K., Pressure sources and induced ground deformation associated with explosive eruptions at an andesitic volcano: Sakurajima, Japan, in *Magma Transport and Storage*, pp. 335-356, John Wiley, New York, 1990.
Jobert, G., Théorie du pendule de Zöllner et du pendule de Lettau, *Geofis. Pura Appl.*, *44*, 25-73, 1959.
Jousset, P., Microgravimétrie et gravimétrie en volcanologie: Méthodologie et application au volcan Merapi, Thèse de Doctorat, 225 pp., Univ. Denis Diderot Paris VII, Paris, 1996.
Jousset, P., S. Dwipa, F. Beauducel, T. Duquesnoy, and M. Diament, Temporal gravity at Merapi during the 1993-1995 crisis: an insight into the dynamical behavior of volcanoes, *J. Volcanol. Geotherm. Res.*, in press, 1998.
Klein, G., and G. Boedecker, GPS-observations in a local network covering big height differences, in *Global Positioning System: an Overview*, *Proc. Symp. IUGG–IAG, Edinburgh*, *102*, 90-94, 1989.
Kofman, W., A. Silvent, and J. Liénard, Étude théorique et expérimentale du corrélofiltre, *Ann. Télécommun.*, *37*, 115-122, 1982.
McTigue, D.F., Elastic stress and deformation near a finite spherical magma body: Resolution of the point source paradox, *J. Geophys. Res.*, *92*, 12931-12940, 1987.
McTigue, D.F., and P. Segall, Displacements and tilts from faults and magma chambers beneath irregular surface topography, *Geophys. Res. Lett.*, *15*, 601-604, 1988.
McTigue, D.F., and R.S. Stein, Topographic amplification of tectonic displacement: implications for geodetic measurement of strain changes, *J. Geophys. Res.*, *89*, 1123-1131, 1984.
Minakami, T., T. Miyazaki, and I. Surjo, Topographical change in the area near the summit crater of Mt. Merapi and its geothermal survey, *Bull. Earthquake Res. Inst. Univ. Tokyo*, *47*, 951-967, 1969.
Mogi, K., Relations between the eruptions of various volcanoes and the deformations of the ground surfaces around them, *Bull. Earthquake Res. Inst. Univ. Tokyo*, *36*, 99-134, 1958.
Mortensen, C.E., and D.G. Hopkins, Tiltmeter measurements in Long Valley Caldera, California, *J. Geophys. Res.*, *92*, 13767-13776, 1987.
Okada, Y., Surface deformation due to shear and tensile faults in a half-space, *Bull. Seismol. Soc. Am.*, *75*, 1135-1154, 1985.
Oppenheim, A.V., and R.W. Schafer, *Discrete-Time Signal Processing*, pp. 311-312, Prentice-Hall, Englewood Cliffs, N.J., 1989.
Ratdomopurbo, A., Étude sismologique du volcan Merapi et formation du dôme de 1994, Thèse de Doctorat, 208 pp., Univ. Joseph Fourier Grenoble I, Grenoble, 1995.
Ratdomopurbo, A., and G. Poupinet, Monitoring a temporal change of seismic velocity in a volcano: Application to the 1992 eruption of Mt. Merapi (Indonesia), *Geophys. Res. Lett.*, *22*, 775-778, 1995.
Saastamoinen, J., Contributions to the theory of atmospheric refraction, *Bull. Geod.*, *105*, 279-298, 1972.
Saleh, B., P.A. Blum, and H. Delorme, New silica compact tiltmeter for deformations measurement, *J. Survey Eng.*, *117*, 27-35, 1991.
Subandriyo, M.A. Purbawinata, M. Iguchi, K. Ishihara, K.D. Young, and B. Voight, Ground deformation measured by tiltmeters at Merapi volcano during the 1992-1994 eruption, paper presented at Merapi Volcano Decade International Workshop, UNESCO-VSI, Yogyakarta, Oct. 1995.
Tarantola, A., *Inverse Problem Theory: Methods for Data Fitting and Model Parameter Estimation*, Elsevier, New York, 1987.
Tjetjep, W.S., and S.R. Wittiri, 75 tahun penyelidikan gunungapi di Indonesia, report Direkt. Vulkanol., Bandung, Indonesia, 1996.
Triplet, J.P., and C. Roche, *Météorologie Générale*, 300 pp., Météo France, Paris, 1983.
U.S. Army Map Service, Java Muntilan 1:50,000, CINCUSAPARAC, Far East, *5020 II*, 1964.
Van Ruymbeke, M., F. Beauducel, and A. Somerhausen, The Environmental Data Acquisition System (EDAS) developed at the Royal Observatory of Belgium, *Cahiers du CEGS Luxembourg*, *14*, 163-174, 1997.
Viodé, J.P., Bulletin mensuel d'activité Observatoire Volcanologique de la Montagne Pelée, report Inst. de Phys. du Globe de Paris, June 1997.
Wolfe, J.E., E. Berg, and G.H. Sutton, The change in strain comes mainly from the rain: Kipapa, Oahu, *Bull. Seismol. Soc. Am.*, *71*, 1625-1635, 1981.

F. Beauducel and F.H. Cornet, Institut de Physique du Globe de Paris, Département de Sismologie, Laboratoire de Mécanique des Roches, 4 Place Jussieu, 75252 Paris Cedex 05, France. (E-mail: beauducel@ipgp.jussieu.fr; cornet@ipgp.jussieu.fr)

(Received December 3, 1997; revised August 18, 1998;
accepted September 15, 1998.)